

Spaced-Antenna Interferometry to Measure Crossbeam Wind, Shear, and Turbulence: Theory and Formulation

GUIFU ZHANG

School of Meteorology, University of Oklahoma, Norman, Oklahoma

RICHARD J. DOVIK

National Severe Storms Laboratory, Norman, Oklahoma

(Manuscript received 11 April 2006, in final form 9 August 2006)

ABSTRACT

The theory of measuring crossbeam wind, shear, and turbulence within the radar's resolution volume V_6 is described. Spaced-antenna weather radar interferometry is formulated for such measurements using phased-array weather radar. The formulation for a spaced-antenna interferometer (SAI) includes shear of the mean wind, allows turbulence to be anisotropic, and allows receiving beams to have elliptical cross sections. Auto- and cross-correlation functions are derived based on wave scattering by randomly distributed particles. Antenna separation, mean wind, shear, and turbulence all contribute to signal decorrelation. Crossbeam wind cannot be separated from shear, and thus crossbeam wind measurements are biased by shear. It is shown that SAI measures an apparent crossbeam wind (i.e., the angular shear of the radial wind component). Whereas the apparent crossbeam wind and turbulence within V_6 cannot be separated using monostatic Doppler techniques, angular shear and turbulence can be separated using the SAI.

1. Introduction

Wind, shear, and turbulence are important in quantifying and forecasting weather. The wind field is measured either by Doppler or interferometric techniques (Doviak and Zrnic 2006; Doviak et al. 1996). Weather radars, such as the Weather Surveillance Radar-1988 Doppler (WSR-88D), measure the Doppler velocity (i.e., the radial component of the scatterers' velocity) and its associated distribution (i.e., the spectrum width). But a spaced-antenna interferometer (SAI) such as the National Center for Atmospheric Research's (NCAR's) Multiple Antenna Profiler Radar (MAPR; Cohn et al. 2001) can, if wind is uniform, also measure the crossbeam wind, as well as the along-beam wind component within the radar's resolution volume V_6 (Doviak and Zrnic 2006, their section 4.4.4). The spaced-antenna method was first applied to the measurement of crossbeam winds in the upper atmosphere

(Mitra 1949; Briggs et al. 1950). Alternatives to direct measurements of crossbeam wind, numerical modeling techniques have been applied to retrieve crossbeam winds (e.g., Gao et al. 2001; Xu et al. 2001; Shapiro et al. 2003) from single-Doppler radar measurements. Sophisticated data assimilation techniques, such as the four-dimensional variational (e.g., Sun and Crook 1997) and ensemble Kalman filter (e.g., Snyder and Zhang 2003; Tong and Xue 2005) methods, are necessary for optimal retrievals. All of these retrieval techniques require multiple volume scans of radial velocity data and often involve a number of assumptions; it is advantageous to have direct measurements of the crossbeam winds, and the SAI is one such instrument that can, under certain limitations discussed in this paper, provide such measurements.

However, applications of the SAI have been limited mainly to long-wavelength (i.e., >6 m) radars for wind measurements in the mesosphere-stratosphere-troposphere (MST), and shorter-wavelength (i.e., 30 cm) boundary layer profiling radars. The theory for these radars has been developed assuming anisotropic Bragg scatterers in uniform mean flow with isotropic turbulence (Briggs 1984; Doviak et al. 1996). Recently,

Corresponding author address: Dr. Guifu Zhang, School of Meteorology, University of Oklahoma, 120 David L. Boren Blvd., Suite 5900, Norman, OK 73072-7307.
E-mail: guzhang1@ou.edu

the SAI technique has received attention by the weather radar community. The MAPR was mounted on a pedestal to form a mechanically scanned beam (Brown et al. 2005). An X-band dual-polarization SAI (DPSA; also with a mechanically scanned beam) has been built and data have been collected with it for crossbeam wind measurement (Hardwick et al. 2005). Neither the scanning MAPR nor the DPSA has produced satisfactory crossbeam wind measurements resulting from various limitations, some of which are addressed herein. Turbulence and shear limit the accurate measurement of crossbeam wind. Turbulence is usually calculated from spectrum width data, which can be corrupted by wind shear (Fang and Doviak 2001; Fang et al. 2004). The effect of shear on crossbeam wind measurement has not been fully understood and is addressed in this paper.

Another fundamental limitation is the requirement of a long dwell time at each beam direction for accurate crossbeam wind measurements using an SAI. This is contrary to the idea of fast-scanning weather radar for large volume coverage. A phased-array weather radar called the National Weather Radar Test Bed (NWRT), located at the National Severe Storms Laboratory (NSSL) in Norman, Oklahoma, offers an opportunity to explore SAI techniques for crossbeam wind measurements using electronically scanned beams. The NWRT was developed by a government–university–industry team consisting of the National Oceanic and Atmospheric Administration’s NSSL, the Tri-Agencies’ (Departments of Commerce, Defense, and Transportation) Radar Operations Center (ROC), the U.S. Navy’s Office of Naval Research, the Lockheed Martin Corporation, the University of Oklahoma’s Electrical and Computer Engineering Department and School of Meteorology, the Oklahoma State Regents for Higher Education, the Federal Aviation Administration’s William J. Hughes Technical Center, and Basic Commerce and Industries, Inc., to facilitate the collaborative study of the phased-array radar (PAR) as a multiuse radar for weather and aviation. The NWRT characteristics are described by Forsyth et al. (2005). The NWRT has a pulse-to-pulse beam-steering capability that provides better utilization of radar resources (Orescanin et al. 2005) so that shorter dwell times for normal weather surveillance can be interlaced with longer ones for weather radar interferometry. Thus, a NWRT-type SAI can simultaneously survey weather and measure crossbeam wind and shear, as well as turbulence along selected directions. A complete theory for such an application has not been developed, although a series of theoretical studies were performed for SAI applications to wind profiling (e.g., Liu et al.

1990; Woodman 1991; Doviak et al. 1996). These studies have been based on the assumption of wave scattering from a statistically homogenous medium of refraction index fluctuations; no shear effects have been accounted, and particle scattering has not been considered.

We formulate the theory of weather radar interferometry for measurements of crossbeam wind, shear, and turbulence for an SAI scanning precipitation. Auto- and cross-correlation functions are derived based on wave scattering by randomly distributed particles. The antenna separation, mean wind, shear, and anisotropic turbulence are all taken into account in the formulation.

This paper is organized as follows. Possible SAI configurations for the NWRT and their use are discussed in section 2. Spaced-antenna interferometry is formulated based on wave scattering from randomly distributed scatterers in section 3; in section 4 the composite of mean crossbeam wind and crossbeam shear of the mean longitudinal wind, the longitudinal wind, and turbulence are estimated from the auto- and cross-correlation functions. The separation of turbulence from wind and shear measurements is discussed in this section.

2. Possible SAI configurations for the NWRT

The NWRT is the first phased-array weather radar operating in the 10-cm-wavelength band (the same as WSR-88Ds). The NWRT has been adapted from a monopulse antenna used for target detection and tracking. The antenna from an AN/SPY-1A radar (Brookner 1988) and a transmitter from a WSR-88D weather radar are used for the NWRT (Fig. 1a). The NWRT transmits with all of the array elements uniformly excited and receives signals with tapered weighting. The antenna has three ports (i.e., a sum, azimuth difference, and elevation difference). Although the antenna’s difference channels were disabled when it was transferred to the National Severe Storms Laboratory in Norman, these channels are presently being activated.

One of the research/development objectives for the NWRT is to make instantaneous and direct measurement of wind components along and across the beam at each V_6 along the beam. The NWRT is capable of providing crossbeam wind and shear measurements *within the beam* while surveying the weather, a capability that does not exist with mechanically steered beams. The NWRT phased-array antenna allows SAI wind measurements without any change to the antenna hardware. The sum and azimuth difference signals can be used to form an azimuth SAI with two virtual receivers,

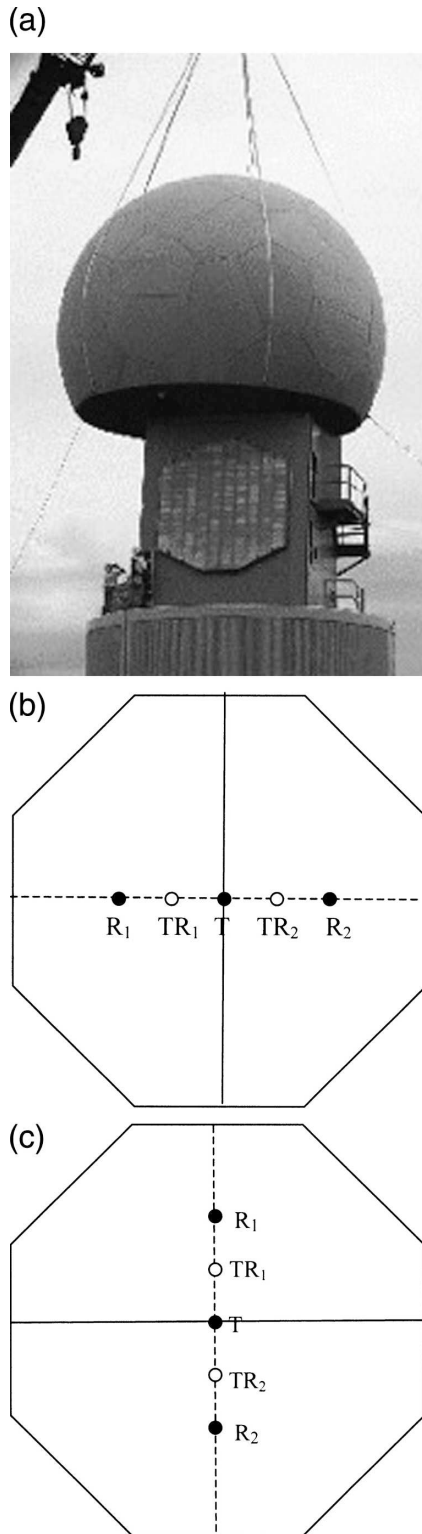


FIG. 1. (a) The NWRT phased-array antenna (photo, courtesy of A. Zahrai, NSSL), and the configuration of receiving apertures R_1 , R_2 for SA weather radar interferometry for (b) azimuth SAI and (c) elevation SAI.

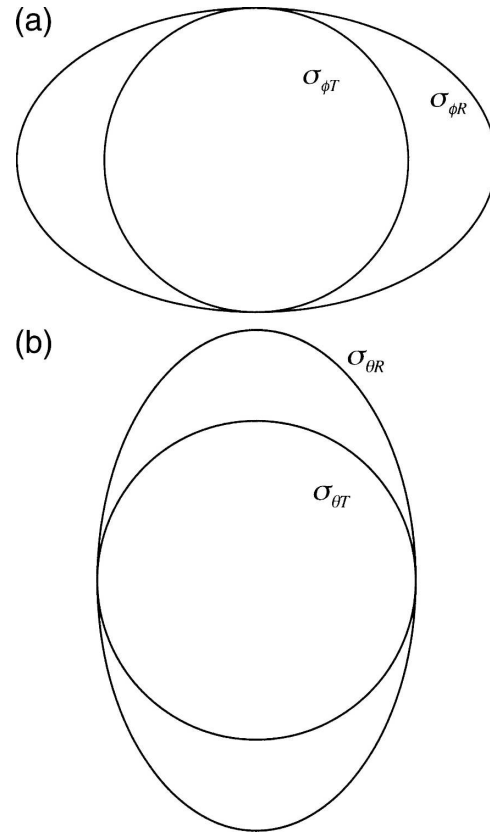


FIG. 2. Sketch of transmitting and receiving antenna beamwidths for the NWRT. The inner circles represent the transmitting beam (also the beam associated with the receiving sum channel), and the outer ellipse is the beam associated with one of the SAI receiving apertures: (a) azimuth SAI and (b) zenith SAI. The theoretical transmitting and receiving beamwidths are $\theta_{1T} = 2.36\sigma_{\theta T} \approx 1.53^\circ$ and $\theta_{1R} = 2.36\sigma_{\theta R} \approx 3.06^\circ$.

one for each of the left and right halves of the antenna, as shown in Fig. 1b. Similarly, an elevation SAI can be constructed (Fig. 1c) from the sum and the elevation difference signals. A PAR in which one has access to many more elements would allow the receiving antennas to be overlapped so that better performance for wind measurements can be achieved in low signal-to-noise environments (Zhang et al. 2004).

The antenna patterns for the monopulse sum and difference channels are shown in Zhang et al. (2005). Here, the beam cross sections for the full and half-receiving apertures are sketched in Fig. 2. Figure 2a shows the full-aperture beam as a circle, and the beam of the azimuth half aperture is shown as an ellipse, corresponding to the azimuth SAI (Fig. 1b). The reduced azimuth resolution is due to the reduced antenna size in the azimuthal direction. Rotating the antenna patterns in Fig. 2a by 90° leads to Fig. 2b, which shows the beam cross sections for the zenith SAI (Fig. 1c).

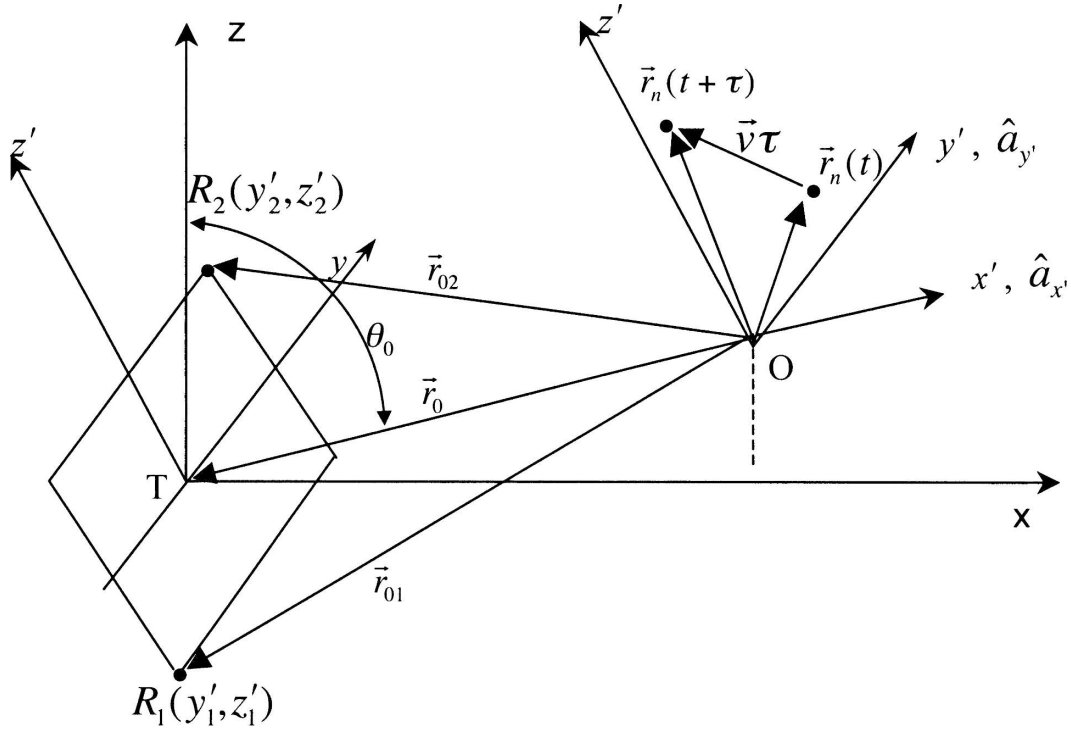


FIG. 3. The coordinate systems and parameters used for SA weather radar interferometry. The phase centers of the SAI receiving and transmitting apertures are R_1 , R_2 , and T , respectively. The beam axis, at a zenith θ_0 , lies in the x, z vertical plane (e.g., the east–west vertical plane). The y', z' plane is tilted and parallel to the plane that contains the receiving and transmitting constant-phase apertures. The origin of the tilted Cartesian coordinate system is at the center of V_6 .

The elliptically shaped cross sections of the receiving antennas' fields of view are taken into account in the following formulation.

3. Formulation for spaced-antenna interferometry

Consider an SAI with the phase center of the transmitting aperture at T and that of the two receiving antennas at R_1 and R_2 (Fig. 3). A local Cartesian coordinate system in which $(\mathbf{a}_{x'}, \mathbf{a}_{y'}, \mathbf{a}_{z'})$ are unit vectors has its origin at the center of V_6 , the radar resolution volume circumscribed by the 6-dB contour of beam and range-weighting functions. The x', z' vertical plane is defined as the one in which the beam lies. The x' axis is along the transmitting beam axis, and a location inside V_6 is $\mathbf{r} = x'\mathbf{a}_{x'} + y'\mathbf{a}_{y'} + z'\mathbf{a}_{z'}$. Although the physical aperture

of the NWRT is on a plane tilted 10° from the vertical, the apertures of constant phase and the plane of phase centers for the transmitting T and receiving R_1 and R_2 antennas are parallel to the $(\mathbf{a}_{z'}, \mathbf{a}_{y'})$ plane, which is tilted relative to the physical aperture. In general, the two receiving antennas are separated by $\Delta\rho(\Delta y'_{12}, \Delta z'_{12})$.

Assume there is a spatial distribution of point scatterers, and that the n th scatterer is located at $\mathbf{r}_n(t)$ at time t . Distances from the scatterer to the transmitting and receiving antennas are $|\mathbf{r}_0 - \mathbf{r}_n|$, $|\mathbf{r}_{01} - \mathbf{r}_n|$, and $|\mathbf{r}_{02} - \mathbf{r}_n|$ respectively. Following previous work (Doviak and Zrníc 2006, their section 4.2; Zhang et al. 2005), we have received signals at R_1 and R_2 expressed by

$$V(\mathbf{r}_{01}, t_1) = \sum_{n=1}^N A_{1n} W_{1n} \exp\{-jk[|\mathbf{r}_0 - \mathbf{r}_n(t_1)| + |\mathbf{r}_{01} - \mathbf{r}_n(t_1)|]\} \quad (1)$$

$$V(\mathbf{r}_{02}, t_2) = \sum_{n=1}^N A_{2n} W_{2n} \exp\{-jk[|\mathbf{r}_0 - \mathbf{r}_n(t_2)| + |\mathbf{r}_{02} - \mathbf{r}_n(t_2)|]\}, \quad (2)$$

where A_{1n} is the prefilter echo amplitude of the n th scatterer located at $\mathbf{r}_n(t_1)$ at time t_1 , \mathbf{r}_{01} is the vector distance from the center of V_6 to the receiver at R_1 , and W_{1n} is a range-dependent weight that is a function of the transmitted pulse width and the receiver filter's bandwidth (Doviak and Zrnic 2006, their section 4.4). Similar definitions apply to (2). Here A_{1n} is proportional to the product of the square root of the power density patterns for the transmitting and receiving antennas. Because the range extent of V_6 is usually small compared to r_0 , the small changes in the weighting func-

tion $W(r)$ resulting from the $1/r_0^2$ factor can be ignored.

Thus, the cross correlation of signals from the two receivers can be written as

$$C_{12}(t_2 - t_1) = \langle V^*(\mathbf{r}_{01}, t_1) V(\mathbf{r}_{02}, t_2) \rangle = C_{12}(\tau), \quad (3)$$

under the assumption that signal statistics are stationary, where the angle brackets indicate time or ensemble averaging, and $t_2 - t_1 \equiv \tau \equiv m\text{PRT} \equiv mT_s$ is the sample time spacing, and $\text{PRT} = T_s$ is the pulse repetition time. Therefore, substituting (1) and (2) into (3), we obtain

$$\begin{aligned} C_{12}(\tau) &= \left\langle \sum_{n=1}^N \sum_{n'=1}^N A_{2n} W_{2n} A_{1n}^* W_{1n}^* \exp\{-jk[|\mathbf{r}_0 - \mathbf{r}_n(t_2)| + |\mathbf{r}_{02} - \mathbf{r}_n(t_2)| - |\mathbf{r}_0 - \mathbf{r}_n(t_1)| - |\mathbf{r}_{01} - \mathbf{r}_n(t_1)|]\} \right\rangle \\ &= \left\langle \sum_{n=1}^N A_{2n} W_{2n} A_{1n}^* W_{1n}^* \exp\{-jk[|\mathbf{r}_0 - \mathbf{r}_n(t + \tau)| + |\mathbf{r}_{02} - \mathbf{r}_n(t + \tau)| - |\mathbf{r}_0 - \mathbf{r}_n(t)| - |\mathbf{r}_{01} - \mathbf{r}_n(t)|]\} \right\rangle \\ &= \left\langle \int n(\mathbf{r}) A_2[\mathbf{r}(t + \tau)] W_2[\mathbf{r}(t + \tau)] A_1^*[\mathbf{r}(t)] W_1^*[\mathbf{r}(t)] \exp\{-jk[|\mathbf{r}_0 - \mathbf{r}(t + \tau)| + |\mathbf{r}_{02} - \mathbf{r}(t + \tau)| - |\mathbf{r}_0 - \mathbf{r}(t)| - |\mathbf{r}_{01} - \mathbf{r}(t)|]\} d\mathbf{r} \right\rangle. \end{aligned} \quad (4)$$

Because scatterers are randomly located and move independently of each other, the expectations of the off-diagonal terms of the matrix are zero (Doviak and Zrnic 2006, their section 5.2.2); thus, the double sum has been reduced in Eq. (4) to a single sum along the matrix diagonal. Furthermore, the weighted sum has

been replaced by the weighted integral of the number density $n(\mathbf{r})$ of scatterers at \mathbf{r} . Henceforth $n(\mathbf{r})$ is assumed to be uniform across V_6 , although it can be a function of V_6 location.

To perform the integral in (4), the angular and range weighting functions are needed; these can be expressed as

$$A_i[\mathbf{r}(t)] = A_0 g_T^{1/2} g_R^{1/2} \exp\left[-\frac{z'^2(t)}{4r_0^2 \sigma_{\theta T}^2} - \frac{[z'(t) - z'_i]^2}{4r_0^2 \sigma_{\theta R}^2} - \frac{y'^2(t)}{4r_0^2 \sigma_{\phi T}^2} - \frac{[y'(t) - y'_i]^2}{4r_0^2 \sigma_{\phi R}^2}\right], \quad (5a)$$

$$W_i[\mathbf{r}(t)] = \exp\left[-\frac{x'^2(t)}{4\sigma_R^2}\right], \quad (5b)$$

where $i = 1, 2$ and (y'_i, z'_i) are the phase centers of the SAI receiving apertures, σ_R^2 is the second central moment of the range-weighting function assumed equal for both receivers, $\sigma_{\theta T}$ and $\sigma_{\theta R}$ are the square roots of the second central moment of the *one-way* power-weighting functions along the zenith for the transmitting and receiving antennas, respectively, and $\sigma_{\phi T}$ and $\sigma_{\phi R}$ are, correspondingly, those beamwidths along the azimuth (Fig. 2). Referenced to the commonly used one-way 3-dB beamwidth, $\theta_{1T} = 2.36\sigma_{\theta T}$, where $\sigma_{\theta T} = \gamma\lambda/D$. Parameters λ , D , and γ are the wavelength, the diameter of the transmitting antenna, and a beamwidth factor (of the order of $1/2$) that depends on the weight-

ing of the aperture elements. We have assumed that the receiving apertures could be located anywhere in the z' , y' plane, although, for the NWRT, the phase centers of the receiving apertures are constrained to lie either along z' (i.e., $\Delta y'_{12} = 0$ for v_z crossbeam wind measurements) or along y' (i.e., $\Delta z'_{12} = 0$ for v_y crossbeam wind measurements). Furthermore, although beamwidths of the NWRT are functions of the angular displacement of the beams relative to the boresight (i.e., the direction perpendicular to the plane of the physical aperture), we shall assume the beam is directed along or near the boresight.

A Taylor series expansion is applied to the phase terms up to the second order in the location $\mathbf{r} = (x', y', z')$ of the elemental scattering volume $d\mathbf{r}$ (Doviak and Zrnic 2006, their section 11.5) to obtain

$$\begin{aligned} |\mathbf{r}_0 - \mathbf{r}(t)| &\approx r_0 + x'(t) + \frac{z'^2(t) + y'^2(t)}{2r_0}; \\ |\mathbf{r}_{01} - \mathbf{r}(t)| &= r_0 + x'(t) + \frac{[z'_1 - z'(t)]^2 + [y'_1 - y'(t)]^2}{2r_0}, \end{aligned} \quad (6)$$

with similar expansions for the other terms in (4) valid for narrow beams. The location of the elemental scattering volume at time $t + \tau$ is

$$\mathbf{r}(t + \tau) = \mathbf{r}(t) + \mathbf{v}\tau, \quad (7)$$

where $\mathbf{v} = v_x \mathbf{a}_{x'} + v_y \mathbf{a}_{y'} + v_z \mathbf{a}_{z'}$ is the velocity of the scatterers within the elemental volume. We assume scatterers are perfect tracers of wind (i.e., inertia effects and terminal velocity are ignored). Strictly speaking, we measure the reflectivity-weighted vertical component of the scatterers' velocity (Doviak and Zrnic 2006, their section 9.2.1). If elevation angles are small, terminal velocities can be ignored; in any case, the azimuthal component of crossbeam wind is not affected by terminal velocity.

Substituting (5)–(7) into (4) yields

$$\begin{aligned} C_{12}(\tau) &= |A_0|^2 n(\mathbf{r}_0) g_{TGR} \left\langle \iiint \exp \left[-\frac{x'^2 + (x' + v_x \tau)^2}{4\sigma_R^2} - \frac{z'^2 + (z' + v_z \tau)^2}{4r_0^2 \sigma_{\theta T}^2} - \frac{(z' - z'_1)^2 + (z' + v_z \tau - z'_2)^2}{4r_0^2 \sigma_{\theta R}^2} \right. \right. \\ &\quad \left. \left. - \frac{y'^2 + (y' + v_y \tau)^2}{4r_0^2 \sigma_{\phi T}^2} - \frac{(y' - y'_1)^2 + (y' + v_y \tau - y'_2)^2}{4r_0^2 \sigma_{\phi R}^2} \right] \right. \\ &\quad \left. \exp \left\{ -jk \left[2v_x \tau + \frac{(z' + v_z \tau)^2 + (z' + v_z \tau - z'_2)^2 - z'^2 - (z' - z'_1)^2}{2r_0} \right. \right. \right. \\ &\quad \left. \left. \left. + \frac{(y' + v_y \tau)^2 + (y' + v_y \tau - y'_2)^2 - y'^2 - (y' - y'_1)^2}{2r_0} \right] \right\} dx' dy' dz' \right\rangle. \end{aligned} \quad (8)$$

The integrations are straightforward for a uniform wind field. If turbulence and shear are present, the velocity is not only random, but its mean is also a function of location. In general, each of the three wind components can have shear in three directions. For narrow beams, motion v_x parallel to the beam axis causes most phase shifts and signal fluctuation; thus, it is justified that only the shears of v_x within V_6 are considered. We assume v_x can be expressed as the Taylor series to first order in \mathbf{r} ,

$$\begin{aligned} v_x(\mathbf{r}) &= v_x(0) + v_{tx} + (\mathbf{s} \cdot \mathbf{r}) \equiv v_{cx} + (\mathbf{s} \cdot \mathbf{r}) \\ &= v_{cx} + s_x x' + s_y y' + s_z z', \end{aligned} \quad (9)$$

where $v_x(0)$ is the mean wind component at the center of V_6 and parallel to the beam axis, v_{tx} is the corresponding turbulent component, v_{cx} is the combined mean and turbulent wind along x' , and $\mathbf{s} = \nabla v_x(\mathbf{r})$ is the

shear assumed uniform across V_6 . Because we only need to consider the shear of the wind parallel to the beam axis, henceforth shear will always refer to the gradient of v_x , unless otherwise noted.

Turbulence \mathbf{v}_t is assumed to be statistically homogeneous, and on average the scatterers' displacements resulting from \mathbf{v}_t are zero. Thus, although the instantaneous turbulent velocity \mathbf{v}_t is a function of \mathbf{r} , turbulence can be treated as a constant independent of the integration variables because, on average, turbulence does not displace the scatterers. Thus, the integration can be performed before the ensemble average. To integrate (8) we combine the mean and turbulent wind components (e.g., v_{cx}); the effect of turbulence becomes apparent after the ensemble average is performed. Substituting (9) into (8), and performing integrations shown in appendix A, we obtain (A4), repeated here as

$$\begin{aligned} C_{12}(\tau) &= |A_0|^2 n(\mathbf{r}_0) g_{TGR} (2\pi)^{3/2} \sigma_R r_0^2 \sigma_{e\theta} \sigma_{e\phi} \exp[-2k^2 \sigma_R^2 s_x^2 \tau^2] \\ &\quad \times \langle \exp[-2jk v_{cx} \tau - 2k^2 \sigma_{e\theta}^2 (r_0 s_z \tau + v_{cz} \tau - \Delta z'_{12}/2)^2 - 2k^2 \sigma_{e\phi}^2 (r_0 s_y \tau + v_{cy} \tau - \Delta y'_{12}/2)^2] \rangle, \end{aligned} \quad (10a)$$

where

$$v_{cx'} = v_x(0) + v_{tx'}, v_{cy'} = v_y(0) + v_{ty'}, v_{cz'} = v_z(0) + v_{tz'} \quad (10b)$$

are the combined mean and turbulent velocities,

$$\Delta y'_{12} = y'_2 - y'_1, \Delta z'_{12} = z'_2 - z'_1 \quad (10c)$$

are the receiving antenna separations in y' and z' directions, and

$$\sigma_{e\theta} = \sqrt{\frac{\sigma_{\theta T}^2 \sigma_{\theta R}^2}{\sigma_{\theta T}^2 + \sigma_{\theta R}^2}}, \sigma_{e\phi} = \sqrt{\frac{\sigma_{\phi T}^2 \sigma_{\phi R}^2}{\sigma_{\phi T}^2 + \sigma_{\phi R}^2}} \quad (10d)$$

define the effective two-way beamwidths in zenith and azimuth, respectively; for the NWRT, $\sigma_{\phi T} = \sigma_{\theta T}$.

Because the SAI can be viewed as a pair of bistatic radars symmetrically located about the transmitter with Fresnel zone centers separated a distance $\Delta y'_{12}/2$ (Doviak et al. 1996), the measured Doppler shift, represented by the phase term in (10a), is proportional to

$$\begin{aligned} C_{12}(\tau) = & |A_0|^2 n(\mathbf{r}_0) g_T g_R 2^{1/2} \pi^{3/2} \sigma_R r_0^2 \sigma_{e\theta} \sigma_{e\phi} \times \exp[-2jkv_{x'}(0)\tau - 2k^2(\sigma_R^2 s_{x'}^2 + \sigma_{ix'}^2)\tau^2] \\ & \times \exp\{-2k^2 \sigma_{e\theta}^2 [r_0 s_{z'} \tau + v_{z'}(0)\tau - \Delta z'_{12}/2]^2 - 2k^2 \sigma_{e\theta}^2 \sigma_{iz'}^2 \tau^2\} \\ & \times \exp\{-2k^2 \sigma_{e\phi}^2 [r_0 s_{y'} \tau + v_{y'}(0)\tau - \Delta y'_{12}/2]^2 - 2k^2 \sigma_{e\phi}^2 \sigma_{iy'}^2 \tau^2\}. \end{aligned} \quad (11)$$

Because the factors $\sigma_{e\theta}$, $\sigma_{e\phi}$ in (11) are much smaller than 1 (for the NWRT $\sigma_{e\theta} \approx 10^{-2}$), the crossbeam components of turbulence typically contribute to signal decorrelation much less than the along-beam component does. On the other hand, if the beam is vertically, or nearly vertically, pointed (as it always is for wind profilers), and if turbulence is anisotropic (e.g., horizontally isotropic with significantly smaller vertical component), crossbeam turbulence could be relatively significant. But, if turbulence is isotropic, or nearly so,

the mean velocity along the bisector of the angle subtended by \mathbf{r}_{01} , \mathbf{r}_{02} . But, because the angle is very small, this phase shift is practically the same as that measured with a monostatic Doppler (e.g., the Doppler shift measured in the sum-receiving channel).

Assuming that turbulent velocity components are independent [i.e., the probability density function satisfies $p(v_{x'}, v_{y'}, v_{z'}) = p(v_{x'})p(v_{y'})p(v_{z'})$], and have a Gaussian probability distribution with standard deviations $\sigma_{ix'}$, $\sigma_{iy'}$ and $\sigma_{iz'}$, the ensemble average can be performed (appendix B). Substituting (B1) to (B3) into (10a), the cross-correlation function can be written as

the contributions of crossbeam turbulence can be ignored as we henceforth assume.

If the receivers are matched and $\Delta z'_{12} = \Delta y'_{12} = 0$, $C_{12}(\tau) \rightarrow C_{11}(\tau) = C_{22}(\tau)$, the autocovariances. At $\tau = 0$, the autocovariance equals the signal power S . Thus,

$$C_{11}(0) = S = |A_0|^2 n(\mathbf{r}_0) g_T g_R (2\pi)^{3/2} \sigma_R r_0^2 \sigma_{e\theta} \sigma_{e\phi}, \quad (12)$$

and the cross-correlation coefficient is

$$\begin{aligned} c_{12}(\tau) \equiv \frac{C_{12}(\tau)}{S} = & \exp(-2jkv_{x'}(0)\tau - 2k^2(\sigma_R^2 s_{x'}^2 + \sigma_{ix'}^2)\tau^2 - 2k^2 \sigma_{e\theta}^2 \{[r_0 s_{z'} + v_{z'}(0)]\tau - \Delta z'_{12}/2\}^2 \\ & - 2k^2 \sigma_{e\phi}^2 \times \{[r_0 s_{y'} + v_{y'}(0)]\tau - \Delta y'_{12}/2\}^2). \end{aligned} \quad (13)$$

If there is no shear, it can be shown that (13) is exactly the same as the cross correlation of signals for Bragg scatter from refractive index perturbations [Doviak et al. 1996, their Eq. (58)], under the condition that the Bragg scatterers' correlation length transverse to the beam is small compared to the antenna diameter (i.e., Bragg scatter is isotropic). Decorrelation of the signal by the mean wind advecting the scatterers out of V_6 is typically small and has been neglected in deriving Eq. (13).

4. Interpretation of the formulation

Equation (13) constitutes the theoretical formulation for SA weather radar interferometry in the presence of mean wind, turbulence, and shear. In using interferom-

etry, we are primarily interested in the magnitudes of the auto- and cross-correlation functions, and henceforth we shall focus on the magnitude of (13). The second and third exponents account for signal decorrelation caused by longitudinal shear $s_{x'}$ and the longitudinal component $\sigma_{ix'}$ of turbulence. The remaining exponents account for signal decorrelation caused by the baseline shear, baseline wind, and receiving antenna separation. Baseline wind and shear are the crossbeam wind and shear parallel to a pair of SAI receivers. As seen from (13), baseline shear combines with baseline wind, and measurements of the correlation functions cannot separate the two.

Because weather radar beamwidths are small, it can be shown that factors $s_{z'} + v_{z'}(0)/r_0 \equiv s_\theta$ and $s_{y'} + v_{y'}(0)/r_0 \equiv s_\phi$ are approximately angular shears of the

mean radial wind. Angular shears are defined as the radial velocity change per differential arc length (e.g., $r_0 \sin\theta_0 d\phi$). Thus, $s_\phi = (1/r_0 \sin\theta_0)(\partial v_r/\partial\phi)$ is the azimuthal angular shear of the radial wind component v_r . Angular shears can also be determined from Doppler measurements at two or more angles in each direction; this measurement is called Doppler beam swinging [DBS; a variant of the velocity–azimuth display (VAD) technique commonly used to determine vector winds from weather observations with a single Doppler radar]. Either the DBS or SAI method can be used to estimate the angular shear of the radial velocity. But, given the same resolution and a high signal-to-noise ratio, the SAI method provides a more accurate measure than the DBS method (Doviak et al. 2004a). The DBS method is employed by wind profilers to measure wind, typically under the assumption that wind is uniform over the region scanned by the beams, and that shear of the vertical wind can be ignored. Ignoring horizontal shear of the vertical wind should be a reasonable assumption for fair weather conditions, but under disturbed conditions this shear could cause significant errors in wind measurements. The effects of shear on wind measurements with profilers was evident in experiments in which six measuring systems were compared; on days of relatively unperturbed flow, estimated winds agreed very well, but the agreement was sporadic on days in which the convective boundary layer was active (Flowers et al. 1994).

As stated above, cross-correlation measurements of weather signals cannot distinguish baseline shear from baseline wind. Thus, shear bias measurements of cross-beam wind are within V_6 . To provide a physical explanation as to why baseline shear acts like baseline wind, consider a pair of scatterers a, b at range r_0 (Fig. 4). The SAI can be viewed as a pair of bistatic radars, TR_1 and TR_2 , symmetrically located about the transmitter T , having phase centers at TR_1 and TR_2 separated by a distance $\Delta y'_{12}/2$ (i.e., the separation of the Fresnel zone centers; Doviak et al. 1996). Fresnel zones are those annuli at range r_0 within which the phase pathlength from T to the scatterer within the annulus and from the scatterer to the receiver remains within $\lambda/2$ for all scatterers within the annulus. Thus, if scatterer “ a ” advects along y' from position a to a' (Fig. 4a), it [or any other scatterer being advected by $v_{y'}(0)$ such as b] will occupy the same relative position within the Fresnel zones of TR_1 , because scatterer a' occupies in the Fresnel zones of TR_2 . Thus, the time series of weather signals from a distribution of scatterers received in bistatic receiver R_2 will be exactly the same as those received in bistatic receiver R_1 , but delayed by $\Delta y'/2v_{y'}(0)$. The key concept is that the phase path $k(Ta' + a'R_2)$ (i.e., from T to

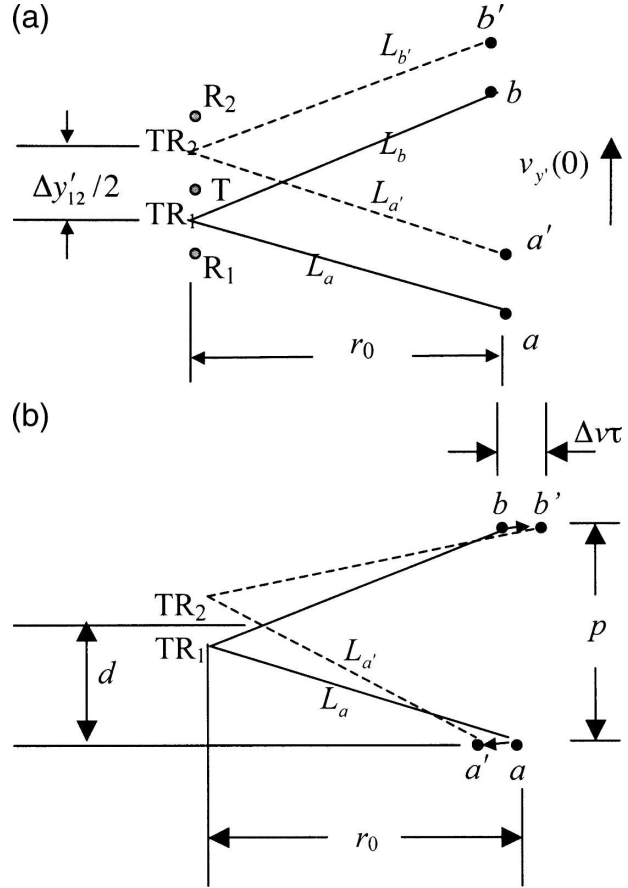


FIG. 4. A bistatic radar schematic to explain how baseline shear acts the same as baseline wind. Time delay caused by (a) cross-beam wind and (b) shear.

a' to R_2), after the scatterer has advected a distance $\Delta y'_{12}/2$, is the same as the initial phase path $k(Ta + a'R_1)$. Alternatively, because $\Delta y'_{12}/2 \ll r_0$, the bistatic radars TR_1, TR_2 can be replaced with a pair of monostatic radars at the respective bistatic phase centers. For example, the DPSA (Hardwick et al. 2005) is a pair of closely spaced monostatic radars. In this case, for signals in receiver R_2 to be identical to those in R_1 after a lag of $\Delta y'/2v_{y'}(0)$, the phase path $kL_{a'}$ needs to be the identical to kL_a .

Now let the scatterers only be moved by shear s_y [i.e., $v_{y'}(0) = 0$; Fig. 4b]. In order for the signal in R_1 to be the same as in R_2 , the paths L_a and $L_{a'}$ must be the same (or equivalently $L_b = L_{b'}$). If the scatterers, spaced p apart, are symmetrically located about the origin, they would be equally displaced $\Delta v\tau$ in opposite directions, where $\Delta v = s_y p/2$. Using the geometry in Fig. 4b,

$$\begin{aligned} L_a &= \sqrt{(d - \Delta y'_{12}/4)^2 + (r_0)^2}; L_{a'} \\ &= \sqrt{(r_0 - \Delta v\tau)^2 + (d + \Delta y'_{12}/4)^2}. \end{aligned} \quad (14)$$

For narrow beams $d \ll r_0$, and typically $d \gg \Delta y'_{12}$, $d \gg \Delta v\tau$. Expanding the radicals to first order in $\Delta v\tau$ and $\Delta y'_{12}$, respectively, and setting $L_a = L_a'$, we obtain

$$\Delta v\tau = \frac{d\Delta y'_{12}}{2r_0}. \quad (15)$$

Substituting $\Delta v = s_y p/2$ and $d/p = 1/2$, the maximum cross correlation of the signals occurs if $r_0 s_y \tau = \Delta x/2$, which is in agreement with that shown by (13).

Equation (13) has also been verified with numerical simulations of wave scattering by a layer of randomly distributed particles moving across the beam (Zhang et al. 2005). Cross-correlation functions are estimated from the simulated time series data. Indeed, the baseline shear of along-beam wind causes the cross-correlation peak to move toward positive or negative time lags, depending on whether shear is positive or negative.

Figure 5 shows the cross-correlation coefficient as a function of τ . The parameters of the NWRT were used for the calculation. Both auto- and cross-correlation coefficients at various ranges are shown in Fig. 5a. At near ranges, signal decorrelation is mainly caused by the antenna separation, crossbeam wind, and turbulence. Previous studies that ignored shear showed that turbulence plays a significant role in decorrelating signals because its effect on the correlation time, compared to that caused by baseline wind, is multiplied by the ratio of the transmitting antenna diameter to wavelength [Doviak et al. 2004b, their Eq. (3)]. But, shear is also a significant factor in decorrelating the signals, especially at long ranges where beamwidths are large. Because σ_R is independent of range, and turbulence is assumed to be uniform, the change in correlation time with range is only due to crossbeam shear.

Figure 5b shows the correlation coefficients for weather signals from scatterers at a fixed range of 30 km, and for various shears along the baseline. Increases of baseline shear not only decrease the correlation time, but it also shifts the time lag to the peak of the cross-correlation function.

Although there appears to be no practical method to separate baseline shear from baseline wind, measurement of the apparent baseline wind [e.g., $v_{ay'}(0) = r_0 s_y' + v_y(0)$], obtained simultaneously everywhere along the beam, might provide useful constraints to sophisticated retrieval algorithms (e.g., Shapiro et al. 2003) that can generate the fields of vector winds over large domains. Henceforth, further discussion is focused on measurements of the apparent baseline wind and turbulence. We need to distinguish a definition of apparent wind used in early observations with SAIs (e.g.,

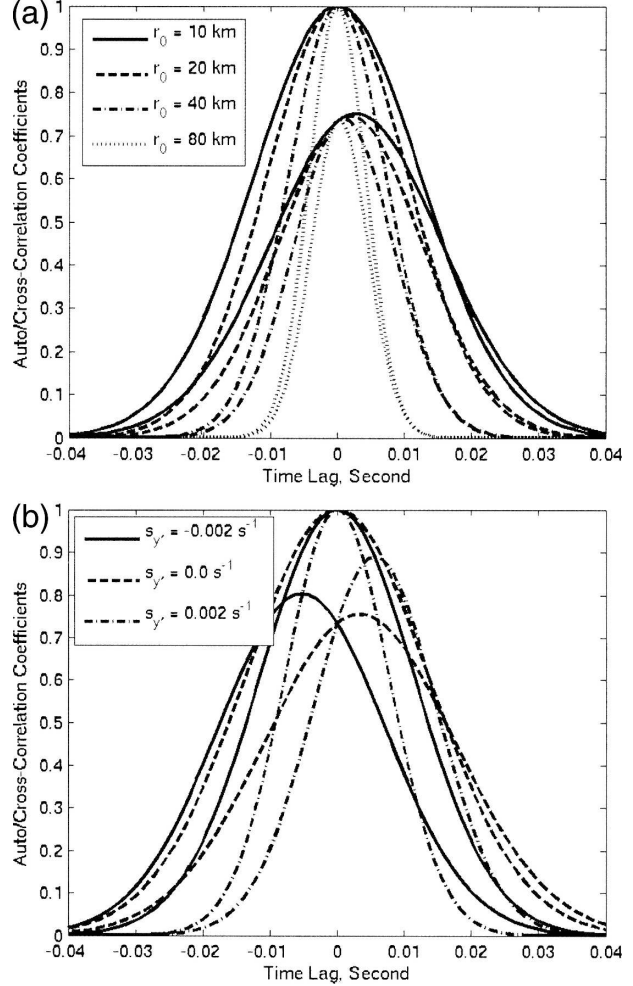


FIG. 5. Auto- and cross-correlation coefficients vs τ at $r_0 = 10, 20, 40,$ and 80 km for NWRT parameters: $\lambda = 0.0938 \text{ m}$, $\Delta y'_{12} = 1.46 \text{ m}$, $\Delta z'_{12} = 0.0 \text{ m}$, $\sigma_{\phi T} = 0.65^\circ$, $\sigma_{\phi R} = 1.30^\circ$. Meteorological parameters are $v_y(0) = 20$, $v_z(0) = 5$, $\sigma_{tx'} = \sigma_{ty'} = \sigma_{tz'} = 0.5 \text{ m s}^{-1}$, and $s_x' = 0$. (a) Dependence on r_0 ; $s_y' = 0$, $s_z' = 0.002 \text{ s}^{-1}$ and (b) dependence on shear s_y' at $r_0 = 30 \text{ km}$; $s_z' = 0.0$.

Briggs 1984). That apparent wind is baseline wind biased by turbulence and/or cross-baseline wind (Holloway et al. 1997), whereas the apparent wind defined herein is baseline wind biased by baseline shear. Apparent baseline winds in this paper are directly related to the angular shears of the radial wind (i.e., $s_\phi = v_{ay'}/r_0$, and $s_\theta = v_{az'}/r_0$).

5. Estimation of the apparent baseline wind and turbulence

a. Estimation of wind

We can calculate the apparent baseline winds from the cross-correlation function using a cross-correlation

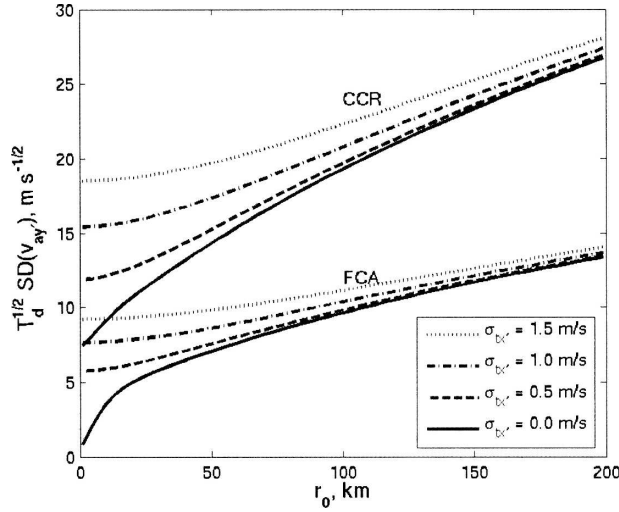


FIG. 6. Normalized standard deviation of apparent wind estimates $\hat{v}_{ay'}(0) = r_0 \hat{s}_{y'} + \hat{v}_{y'}(0)$ vs range for various levels of turbulence and NWR parameters: $\lambda = 0.0938 \text{ m}$, $\Delta y'_{12} \approx 1.46 \text{ m}$, $\Delta z'_{12} = 0.0 \text{ m}$, $\sigma_{\phi T} = 0.65^\circ$, $\sigma_{\phi R} = 1.30^\circ$. The mean apparent baseline wind is $v_{ay'}(0) = 20 \text{ m s}^{-1}$. Other meteorological parameters are $v_x(0) = 0$, $v_z(0) = 5 \text{ m s}^{-1}$, $s_x = 0$, $s_z = 0.002 \text{ s}^{-1}$.

ratio (CCR) method (Zhang et al. 2003), or the full-correlation analysis (FCA) method (Briggs 1984). For example, the apparent azimuth baseline wind component [i.e., $v_{ay'}(0)$] can be calculated from the cross-correlation function for signals from SAI's azimuth receivers (Fig. 1b) for which $\Delta z'_{12} = 0$ in (13). The logarithm of the cross-correlation magnitudes at equal positive and negative lags leads to

$$L_\phi(\tau) = \ln \frac{|c_{12}^{(\phi)}(\tau)|}{|c_{12}^{(\phi)}(-\tau)|} = 4k^2 \sigma_{e\phi}^2 \Delta y'_{12} v_{ay'}(0) \tau. \quad (16)$$

Thus, the apparent baseline wind $v_{ay'}(0)$ is given by

$$v_{ay'}(0) = \frac{L_\phi(\tau)}{4k^2 \sigma_{e\phi}^2 \Delta y'_{12} \tau}. \quad (17)$$

In a similar way, if two SAI-receiving antennas are separated in the zenith direction, the apparent baseline wind component $v_{az'}(0)$ can be calculated. Hence, angular shears s_θ and s_ϕ within V_6 are obtained.

Because baseline shear combines with baseline wind, the accuracies of measuring the *apparent* baseline wind (or angular shear) can be directly derived from theoretical error analysis developed for baseline wind measurements in the absence of shear (e.g., Zhang et al. 2004; Doviak et al. 2004b). Figure 6 shows the standard deviation of the estimates of the apparent azimuthal baseline wind as a function of range and turbulence. The error increase with range is due to the increased

effect of the vertical shear. Compared to measurements of the along-beam wind component using Doppler measurements, baseline wind measurement requires longer dwell times. For example, if the turbulence $\sigma_{lx'} = 0.5 \text{ m s}^{-1}$, about 5 s of data collection time is required to achieve an azimuthal apparent baseline wind $v_{ay'}(0)$, with a measurement accuracy of 2.0 m s^{-1} using the NWR at near ranges. On the other hand, Doppler velocity (i.e., the radial wind component) can be measured with accuracies better than 1 m s^{-1} in a collection time two orders of magnitude shorter. The crossbeam wind estimated using DBS is degraded by a factor of $1/\Delta\theta$, where $\Delta\theta$ is the angular separation, leading to poor measurement accuracy.

b. Estimation of turbulence: The SAI method

Turbulence can be estimated from spectrum width (or, equivalently, the correlation time of the autocorrelation function) using single-beamwidth (1BW) Doppler weather radars such as WSR-88D. Such an estimation is neither accurate nor reliable because beam broadening and shear (Doviak and Zrnicek 2006, their section 5.3) bias the turbulence estimates. Melnikov et al. (2003) show that layers of unusually large spectrum widths (e.g., larger than 8 m s^{-1}), suggestive of turbulence hazardous to safe flight (Lee 1977), are seen in stratiform precipitation. But, these large widths are principally due to shear, and are not necessarily hazardous to safe flight. It is difficult to separate between the shear and turbulence contributions to spectrum width, especially if strong shear is confined to layers that are thin compared to V_6 . Thus, finding an accurate way to estimate turbulence could be advantageous. With the SAI method, turbulence can be calculated from (13), as also shown by Holloway et al. (1997).

Examination of (13) also shows that longitudinal shear s_x combines with turbulence $\sigma_{lx'}$ and thus turbulence measurements are biased by s_x . Because range resolution is fine, longitudinal shear is typically small compared to turbulence and often can be neglected. If not, methods must be found to separate the two. For example, the longitudinal shear s_x can be determined by using different range resolutions, and thus measurements of turbulence can be extracted from (13). But baseline shear cannot be determined by using different beamwidths. Comparisons between turbulence measurements using the SAI method and ones obtained using a beam sufficiently narrow that the transverse shear of the radial wind can be ignored showed good agreement (Chau et al. 2000), confirming the robustness of the SAI method for the measurement of turbulence.

c. The dual-beamwidth method

Recently, a dual-beamwidth (2BW) radar method was applied to a VHF (i.e., 6-m wavelength) profiling radar to measure turbulence using the DBS method (VanZandt et al. 2002). The dual-beamwidth method separates the effect that vertical shear of the horizontal wind has on turbulence measurements when off-vertical beams are used. Off-vertical beams are required at long wavelengths, because vertical incidence backscatter from Bragg scatterers, with correlation lengths not significantly smaller than the antenna diameter, introduces an unknown multiplicative factor that combines with turbulence σ_t (Chau et al. 2000). The use of an off-vertical beam mitigates the backscatter from Bragg scatterers of unknown correlation lengths. Here, we extend the dual-beamwidth method to an anisotropic

beam pattern to estimate shear and turbulence with a weather radar interferometer.

Dual-beamwidth signals are indeed obtained from the NWRT SAI (i.e., the sum channel gives a narrow-beamwidth signal, and each half of the receiving apertures gives broad-beamwidth signals). Thus, by letting $\Delta y'_{12} = \Delta z'_{12} = 0$ and applying (13) to the sum channel, the narrow-beam autocorrelation coefficient magnitude is

$$|c_N(\tau)| \equiv |c_{ss}(\tau)| = \exp[-2k^2\sigma_{ix'}^2\tau^2 - k^2r_0^2\sigma_{\theta T}^2(s_\theta^2 + s_\phi^2)\tau^2]. \quad (18)$$

To obtain a measurement of the angular shear s_ϕ we use the azimuth SAI to obtain the azimuth broad-beam autocorrelation coefficient

$$c_B(\tau)|_\phi = |c_{11}(\tau)| = \exp[-2k^2\sigma_{ix'}^2\tau^2 - k^2r_0^2\sigma_{\theta T}^2(s_\theta\tau)^2 - 2k^2r_0^2\sigma_{e\phi}^2(s_\phi\tau)^2]. \quad (19)$$

To arrive at (19) we substituted $\sigma_{e\theta} = \sigma_{\theta T}/\sqrt{2}$ because, for the azimuth SAI, $\sigma_{\theta R} = \sigma_{\theta T}$. In deriving these two equations we have assumed that longitudinal shear is negligible but, if is not, it can be determined as pointed out in the previous section. Using (18) and (19) s_ϕ^2 is calculated to be

$$s_\phi^2 = \frac{1}{k^2r_0^2\tau^2(2\sigma_{e\phi}^2 - \sigma_{\theta T}^2)} \ln \left[\frac{|c_N(\tau)|}{|c_B(\tau)|_\phi} \right]. \quad (20)$$

Likewise, we can solve for the within-beam shear s_θ in the zenith direction. These two shear values, substituted into (18), lead to the solution

$$\sigma_{ix'}^2 = \frac{1}{2k^2\tau^2} \left\{ \frac{\sigma_{\theta T}^2}{2\sigma_{e\theta}^2 - \sigma_{\theta T}^2} \ln \left[\frac{|c_B(\tau)|_\theta}{|c_N(\tau)|} \right] + \frac{\sigma_{\phi T}^2}{2\sigma_{e\phi}^2 - \sigma_{\theta T}^2} \ln \left[\frac{|c_B(\tau)|_\phi}{|c_N(\tau)|} \right] - \ln |c_N(\tau)| \right\} \quad (21)$$

for turbulence in terms of the measured autocorrelation functions of signals received through the broad azimuth and zenith beams, and the narrow sum beam of the NWRT. These results reduce to those of VanZandt et al. (2002). When s_θ and s_ϕ are calculated, these values are substituted into (19) to obtain a measure of turbulence $\sigma_{ix'}$. In the typical case that azimuthal shear s_ϕ is negligible compared to zenith (i.e., vertical) shear, the second term in (21) can be ignored. Thus, dual-beamwidth-derived shear and turbulence can be compared with those estimated using SA interferometry.

6. Summary and conclusions

We develop and discuss weather radar interferometry to measure, with a spaced-antenna interferometer (SAI), crossbeam wind, turbulence, and shear within the radar's resolution volume V_6 . Although the SAI has principally been applied to measurements of the cloud-free atmosphere, it has potential application to future weather radars. We formulate the problem based on

scattering from randomly distributed particles, allow the receiving beams to have elliptical cross sections (required if full receiving apertures are used), and consider anisotropic turbulence and shear, whereas previous formulations assumed Bragg scatter, circular beams, uniform wind, and isotropic turbulence. Cross- and autocorrelation functions of the weather signals received by a pair of SAI receivers are derived. If turbulence is isotropic the theory shows that turbulence transverse to the beam contributes negligibly to the correlation functions.

It is shown that mean baseline wind (i.e., the cross-beam wind parallel to the baseline connecting a pair of SAI receivers) within V_6 cannot be separated from baseline shear of the mean longitudinal (i.e., along the beam) wind. That is, baseline wind and shear combine to form the angular shear of the radial velocity. Nevertheless, the SAI can separate turbulence from shear within V_6 , whereas this separation cannot be made using Doppler techniques. SAI turbulence measure-

ments could improve quantification of atmospheric turbulent kinetic energy and measurements of turbulence within V_6 .

Meteorologists have been developing methods whereby crossbeam winds can be retrieved from Doppler weather radar data combined with numerical weather models (e.g., Gao et al. 2001; Shapiro et al. 2003). These researchers demonstrate that the retrieval of crossbeam winds from dynamic models is improved if there are observational constraints (e.g., actual measurements of the radial component of wind) in addition to those imposed by the model. For example, a velocity volume processing (VVP; Waldteufel and Corbin 1979) method has been used to estimate the crossbeam wind at selected regions and is added as a constraint to improve the accuracy of the retrieved winds (Shapiro et al. 2003). It is suggested that SAI simultaneous measurements of the angular shear along the beam at chosen beam directions could provide additional observational constraints on the numerically derived wind field. But,

angular shear measurement with SAI requires long dwell times, whereas DBS methods (e.g., the VVP) can make this measurement, albeit with less resolution, in an order or two less dwell time.

Acknowledgments. The authors greatly appreciate helpful discussions with Drs. D. S. Zrnić, Q. Xu, and D. Forsyth of the National Severe Storms Laboratory, and Drs. M. Xue, R. Palmer, and H. Bluestein of the University of Oklahoma. Many thanks go to Lockheed Martin and NSSL's engineers for developing the NWRT. This work was partially supported by NOAA/NSSL under the Cooperative Agreement NA17RJ1227.

APPENDIX A

Integrations over Radar Resolution Volume

To complete the integrations in (8), we perform the integrals over x' first, defining

$$\begin{aligned}
 J_{x'} &= \int \exp\left[-\frac{x'^2 + (x' + v_{cx'}\tau)^2}{4\sigma_R^2} - 2jkv_{cx'}\tau\right] dx' \\
 &= \int \exp\left[-\frac{x'^2 + (x' + v_{cx'}\tau + s_x x'\tau + s_z z'\tau + s_y y'\tau)^2}{4\sigma_R^2} - 2jk(v_{cx'}\tau + s_x x'\tau + s_z z'\tau + s_y y'\tau)\right] dx' \\
 &= \sqrt{\frac{4\pi\sigma_R^2}{1 + (1 + s_x\tau)^2}} \exp\left[-\frac{(v_{cx'}\tau + s_z z'\tau + s_y y'\tau)^2}{4\sigma_R^2} - 2jk(v_{cx'}\tau + s_z z'\tau + s_y y'\tau)\right] \\
 &\quad \times \exp\left\{\frac{[-4jk\sigma_R^2 s_x \tau + (1 + s_x\tau)(v_{cx'} + s_z z' + s_y y')\tau]^2}{4\sigma_R^2[1 + (1 + s_x\tau)^2]}\right\} \sqrt{2\pi\sigma_R} \\
 &\quad \times \exp\left[-\frac{(v_{cx'}\tau + s_z z'\tau + s_y y'\tau)^2}{4\sigma_R^2} - 2jk(v_{cx'}\tau + s_z z'\tau + s_y y'\tau)\right] \exp\left\{\frac{[-4jk\sigma_R^2 s_x \tau + (v_{cx'} + s_z z' + s_y y')\tau]^2}{8\sigma_R^2}\right\} \\
 &\approx \sqrt{2\pi\sigma_R} \exp[-2k^2\sigma_R^2 s_x^2 \tau^2 - 2jk(v_{cx'}\tau + s_z z'\tau + s_y y'\tau)]. \tag{A1}
 \end{aligned}$$

Two assumptions, $s_x\tau \ll 1$ and $[(v_{cx'} + s_z z' + s_y y')^2 \tau^2 / 8\sigma_R^2] \ll 1$, were made in arriving at (A1); these assumptions should be valid for weather radar applications. For example, consider $\tau = p\tau_c$, where τ_c is the correlation time of weather signals and p is a multiplying factor. Typically, correlation functions only have significant values if τ is 2 or 3 times τ_c . For a 10-cm-wavelength radar, $\tau_c \leq 0.02$ s (i.e., spectrum widths $\sigma_v = \lambda/4\pi\tau_c$ are typically larger than 0.5 m s⁻¹). Thus, if $s_x \leq$

20 m s⁻¹ km⁻¹, a rather large value results, $s_x\tau \leq 10^{-3}$. Further argument can be made to show that if beamwidths are less than a few kilometers across, range resolution is about 100 m, and $v_{cx'} \leq 100$ m s⁻¹, the second assumption is acceptable.

If receiving antennas are symmetrically located about the transmitting antenna, the z' integration in (8) can be written as

$$J_z = \int \exp\left[-\frac{z'^2 + (z' + v_{cz'}\tau)^2}{4r_0^2\sigma_{\theta T}^2} - \frac{(z' - z'_1)^2 + (z' + v_{cz'}\tau - z'_2)^2}{4r_0^2\sigma_{\theta R}^2} - 2jks_z z'\tau - \frac{jk}{2r_0}(2z' + v_{cz'}\tau)(2v_{cz'}\tau - \Delta z'_{12})\right] dz',$$

where $\Delta z'_{12} = z'_2 - z'_1$. Carrying out the integration, we arrive at

$$= \sqrt{\pi} \left(\frac{1}{2r_0^2 \sigma_{\theta T}^2} + \frac{1}{2r_0^2 \sigma_{\theta R}^2} \right)^{-1/2} \exp \left[-\frac{v_{cz'}^2 \tau^2}{2} \left(\frac{1}{2r_0^2 \sigma_{\theta T}^2} + \frac{1}{2r_0^2 \sigma_{\theta R}^2} \right) - \frac{z_1'^2 + z_2'^2 - 2z_2' v_{cz'} \tau}{4r_0^2 \sigma_{\theta R}^2} - \frac{jk}{2r_0} v_{cz'} \tau (2v_{cz'} \tau - \Delta z'_{12}) \right] \\ \times \exp \left\{ \left[-jks_{z'} \tau - \frac{jk}{2r_0} (2v_{cz'} \tau - \Delta z'_{12}) - \frac{v_{cz'} \tau}{2} \left(\frac{1}{2r_0^2 \sigma_{\theta T}^2} + \frac{1}{2r_0^2 \sigma_{\theta R}^2} \right) \right]^2 / \left(\frac{1}{2r_0^2 \sigma_{\theta T}^2} + \frac{1}{2r_0^2 \sigma_{\theta R}^2} \right) \right\}.$$

Under far-field conditions (i.e., $r_0 > 2D^2/\lambda$) and similar assumptions used to arrive at (A1), it can be shown the above expression reduces to

$$\approx \sqrt{2\pi} \sigma_{e\theta} r_0 \exp[-2k^2 \sigma_{e\theta}^2 (r_0 s_{z'} \tau + v_{cz'} \tau - \Delta z'_{12}/2)^2 - jks_{z'} \tau v_{cz'} \tau], \tag{A2a}$$

where the effective beamwidth $\sigma_{e\theta}$ is

$$\sigma_{e\theta} = \sqrt{1 / \left(\frac{1}{\sigma_{\theta T}^2} + \frac{1}{\sigma_{\theta R}^2} \right)} = \sqrt{\frac{\sigma_{\theta T}^2 \sigma_{\theta R}^2}{\sigma_{\theta T}^2 + \sigma_{\theta R}^2}}. \tag{A2b}$$

Similarly, we have

$$J_{y'} = \int \exp \left[-\frac{y'^2 + (y' + v_{cy'} \tau)^2}{4r_0^2 \sigma_{\phi T}^2} - \frac{(y' - y'_1)^2 + (y' + v_{cy'} \tau - y'_2)^2}{4r_0^2 \sigma_{\phi R}^2} - 2jks_{y'} y' \tau - \frac{jk}{2r_0} (2y' + v_{cy'} \tau) (2v_{cy'} \tau - \Delta y'_{12}) \right] dy' \\ \approx \sqrt{2\pi} \sigma_{e\phi} r_0 \exp[-2k^2 \sigma_{e\phi}^2 r_0 (r_0 s_{y'} \tau + v_{cy'} \tau - \Delta y'_{12}/2)^2 - jks_{y'} \tau v_{cy'} \tau], \tag{A3a}$$

with

$$\sigma_{e\phi} = \sqrt{\frac{\sigma_{\phi T}^2 \sigma_{\phi R}^2}{\sigma_{\phi T}^2 + \sigma_{\phi R}^2}}. \tag{A3b}$$

Substituting (A1)–(A3) into (8), we obtain

$$C_{12}(\tau) = |A_0|^2 n(\mathbf{r}_0) g_T g_R (2\pi)^{3/2} \sigma_R r_0^2 \sigma_{e\theta} \sigma_{e\phi} \exp[-2k^2 \sigma_R^2 s_x'^2 \tau^2] \\ \times \langle \exp[-2jkv_{cx'} \tau - 2k^2 \sigma_{e\theta}^2 (r_0 s_{z'} \tau + v_{cz'} \tau - \Delta z'_{12}/2)^2 - 2k^2 \sigma_{e\phi}^2 (r_0 s_{y'} \tau + v_{cy'} \tau - \Delta y'_{12}/2)^2] \rangle. \tag{A4}$$

APPENDIX B

Ensemble Average Velocity Fluctuations

The three components $v_{ix'}$, $v_{iy'}$, $v_{iz'}$ of turbulence are assumed to be independent [i.e., $p(v_{ix'}, v_{iy'}, v_{iz'}) = p(v_{ix'}) p(v_{iy'}) p(v_{iz'})$], and each has a Gaussian-shaped probability distribution with, in general, different rms values $\sigma_{ix'}$, $\sigma_{iy'}$, $\sigma_{iz'}$; that is, we allow turbulence to be

anisotropic. Substituting (11) into (10a), the ensemble average over the three components of turbulence reduces to the product $I_x' I_y' I_z'$, where I_x' is defined as

$$I_x' \equiv \langle \exp(-2jkv_{cx'} \tau) \rangle.$$

Because only $v_{ix'}$ is a random variable, the above equation can be expressed as

$$\begin{aligned}
 I_{x'} &= \exp[-2jkv_{x'}(0)\tau] \langle \exp(-2jkv_{ix'}\tau) \rangle \\
 &= \exp[-2jkv_{x'}(0)\tau] \int \exp(-2jkv_{ix'}\tau) p(v_{ix'}) dv_{ix'} \\
 &= \frac{1}{\sqrt{2\pi\sigma_{ix'}}} \exp[-2jkv_{x'}(0)\tau] \int \exp(-2jkv_{ix'}\tau) \exp\left(-\frac{v_{ix'}^2}{2\sigma_{ix'}^2}\right) dv_{ix'}.
 \end{aligned}$$

Performing the integration, we obtain

$$I_{x'} = \exp[-2jkv_{x'}(0)\tau] \exp(-2k^2\sigma_{ix'}^2\tau^2). \quad (B1)$$

Now turning our attention to the crossbeam terms,

$$\begin{aligned}
 I_{z'} &= \langle \exp[-k^2\sigma_{e\theta}^2(r_0s_{z'}\tau + v_{cz'}\tau - \Delta z'_{12}/2)^2] \rangle = \langle \exp\{-2k^2\sigma_{e\theta}^2[r_0s_{z'}\tau + v_{z'}(0)\tau + v_{iz'}\tau - \Delta z'_{12}/2]^2\} \rangle \\
 &= \int \exp[-2k^2\sigma_{e\theta}^2(r_0s_{z'}\tau + v_{z'}(0)\tau + v_{iz'}\tau - \Delta z'_{12}/2)^2] p(v_{iz'}) dv_{iz'} \\
 I_{z'} &= \frac{1}{\sqrt{2\pi\sigma_{iz'}}} \int \exp\{-2k^2\sigma_{e\theta}^2[r_0s_{z'}\tau + v_{z'}(0)\tau + v_{iz'}\tau - \Delta z'_{12}/2]^2\} \exp\left(-\frac{v_{iz'}^2}{2\sigma_{iz'}^2}\right) dv_{iz'}.
 \end{aligned}$$

Performing the integration, we obtain

$$\begin{aligned}
 I_{z'} &= \frac{1}{(1 + 4k^2\sigma_{e\theta}^2\sigma_{iz'}^2\tau^2)^{1/2}} \exp\left\{ \frac{8\sigma_{iz'}^2}{1 + 4k^2\sigma_{e\theta}^2\sigma_{iz'}^2\tau^2} k^4\sigma_{e\theta}^4\tau^2[r_0s_{z'}\tau + v_{z'}(0)\tau - \Delta z'_{12}/2]^2 \right\} \\
 &\quad \times \exp\{-2k^2\sigma_{e\theta}^2[r_0s_{z'}\tau + v_{z'}(0)\tau - \Delta z'_{12}/2]^2\}.
 \end{aligned}$$

Because $2k^2\sigma_{e\theta}^2\sigma_{iz'}^2\tau^2 \ll 1$ for typical weather radar parameters, we convert the square root factor in the denominator to an exponential function, and by keeping terms to second order in τ^2 , this equation can be expressed more simply as

$$\approx \exp\{-2k^2\sigma_{e\theta}^2[r_0s_{z'}\tau + v_{z'}(0)\tau - \Delta z'_{12}/2]^2 - 2k^2\sigma_{e\theta}^2\sigma_{iz'}^2\tau^2\}. \quad (B2)$$

In a like procedure, the integral $I_{y'}$ is

$$\begin{aligned}
 I_{y'} &= \langle \exp\{-2k^2\sigma_{e\phi}^2[r_0s_{y'}\tau + v_{y'}(0)\tau + v_{iy'}\tau - \Delta y'_{12}/2]^2\} \rangle \\
 &= \int \exp\{-2k^2\sigma_{e\phi}^2[r_0s_{y'}\tau + v_{y'}(0)\tau + v_{iy'}\tau - \Delta y'_{12}/2]^2\} p(v_{iy'}) dv_{iy'} \\
 &\approx \exp\{-2k^2\sigma_{e\phi}^2[r_0s_{y'}\tau + v_{y'}(0)\tau - \Delta y'_{12}/2]^2 - 2k^2\sigma_{e\phi}^2\sigma_{iy'}^2\tau^2\}.
 \end{aligned} \quad (B3)$$

REFERENCES

Briggs, B. H., 1984: The analysis of spaced sensor data by correlation techniques. MAP Handbook, Vol. 13, SCOSTEP Secretariat, University of Illinois at Urbana-Champaign, 166-186.

—, G. J. Phillips, and D. H. Shinn, 1950: The analysis of observations on spaced receivers of the fading radio signals. *Proc. Phys. Soc. London*, **63B**, 106-121.

Brookner, E., 1988: *Aspects of Modern Radar*. Artech House, 574 pp.

Brown, W., G. Zhang, T.-Y. Yu, and S. Cohn, 2005: A demonstration of a scanning multiple antenna UHF radar. Preprints,

32nd Conf. on Radar Meteorology, Albuquerque, NM, Amer. Meteor. Soc., CD-ROM, 12R.13.

Chau, J. L., R. J. Doviak, A. Muchinski, and C. L. Holloway, 2000: Tropospheric measurements of turbulence and characteristics of Bragg scatterers using the Jicamarca VHF radar. *Radio Sci.*, **35**, 179-193.

Cohn, S. A., W. O. J. Brown, C. L. Martin, M. S. Susedik, G. Maclean, and D. B. Parsons, 2001: Clear air boundary layer spaced antenna wind measurement with the Multiple Antenna Profiler (MAPR). *Ann. Geophys.*, **19**, 845-854.

Doviak, R. J., and D. S. Zrnica, 2006: *Doppler Radar and Weather Observations*. Dover, 562 pp.

- , R. J. Lataitis, and C. L. Holloway, 1996: Cross correlation and cross spectra for spaced antenna wind profilers: 1. Theoretical analysis. *Radio Sci.*, **31**, 157–180.
- , G. Zhang, S. A. Cohn, and W. O. J. Brown, 2004a: Comparison of Doppler beam swinging and spaced antenna radars for wind measurement; theory. *Int. Union of Radio Science National Radio Science Meeting*, Boulder, CO, URSI, 143.
- , —, —, and W. Brown, 2004b: Comparison of spaced-antenna wind estimators: Theoretical and simulation results. *Radio Sci.*, **39**, 1006, doi:10.1029/2003RS002931.
- Fang, M., and R. J. Doviak, 2001: Spectrum width statistics of various weather phenomena. National Severe Storms Laboratory Rep., 62 pp.
- , —, and V. Melnikov, 2004: Spectrum width measured by WSR-88D: Error sources and statistics of various weather phenomena. *J. Atmos. Oceanic Technol.*, **21**, 888–904.
- Flowers, W., L. Parker, G. Hoidale, E. Santantonio, and J. Hines, 1994: Evaluation of a 924 MHz wind profiling radar. Army Research Laboratory Final Rep. ARL-CR-101, CD-ROM.
- Forsyth, D., and Coauthors, 2005: The National Weather Radar Testbed (Phased-Array). Preprints, *32d Conf. on Radar Meteorology*, Albuquerque, NM, Amer. Meteor. Soc., CD-ROM, 12R.3.
- Gao, J., M. Xue, A. Shapiro, Q. Xu, and K. K. Droegemeier, 2001: Three-dimensional simple adjoint velocity retrievals from single Doppler radar. *J. Atmos. Oceanic Technol.*, **18**, 26–38.
- Hardwick, K. M., S. J. Frazier, and A. L. Pazmany, 2005: Spaced antenna measurements of crossbeam velocity in severe storms. Preprints, *32d Int. Conf. on Radar Meteorology*, Albuquerque, NM, Amer. Meteor. Soc., CD-ROM, P4R.11.
- Holloway, C. L., R. J. Doviak, S. A. Cohn, R. J. Lataitis, and J. S. Van Baelen, 1997: Cross correlations and cross spectra for spaced antenna wind profilers, 2. Algorithms to estimate wind and turbulence. *Radio Sci.*, **32**, 967–982.
- Lee, J. T., 1977: Applications of Doppler radar to turbulence measurements which affect aircraft. FAA System Research Development Service Final Rep. FAA-RD-77-145, 52 pp.
- Liu, C. H., J. Röttger, C. J. Pan, and S. J. Franke, 1990: A model for spaced-antenna observational mode for MST radars. *Radio Sci.*, **25**, 551–563.
- Melnikov, V. M., R. J. Doviak, and M. Fang, 2003: Radar observations of turbulence and wind shear. Preprints, *31st Conf. on Radar Meteorology*, Seattle, WA, Amer. Meteor. Soc., CD-ROM, 9B.5.
- Mitra, S. N., 1949: A radio method of measuring winds in the ionosphere. *Proc. Inst. Electron. Eng.*, **96**, 441–446.
- Orescanin, M., T.-Y. Yu, C. D. Curtis, D. S. Zrnic, and D. Forsyth, 2005: Signal processing of beam-multiplexed data for phased-array weather radar. Preprints, *32d Int. Conf. on Radar Meteorology*, Albuquerque, NM, Amer. Meteor. Soc., CD-ROM, 4R.6.
- Shapiro, A., P. Robinson, J. Wurman, and J. Gao, 2003: Single-Doppler velocity retrieval with rapid-scan radar data. *J. Atmos. Oceanic Technol.*, **20**, 1758–1775.
- Snyder, C., and F. Zhang, 2003: Assimilation of simulated Doppler radar observations with an ensemble Kalman filter. *Mon. Wea. Rev.*, **131**, 1663–1677.
- Sun, J., and N. A. Crook, 1997: Dynamical and microphysical retrieval from Doppler radar observations using a cloud model and its adjoint. Part I: Model development and simulated data experiments. *J. Atmos. Sci.*, **54**, 1642–1661.
- Tong, M., and M. Xue, 2005: Ensemble Kalman filter assimilation of Doppler radar data with a compressible nonhydrostatic model: OSS experiments. *Mon. Wea. Rev.*, **133**, 1789–1807.
- VanZandt, T. E., G. D. Nastrom, J. Furumoto, T. Tsuda, and W. L. Clark, 2002: A dual-beamwidth radar method for measuring atmospheric turbulent kinetic energy. *Geophys. Res. Lett.*, **29**, 1572, doi:10.1029/2001GL014283.
- Waldteufel, P., and H. Corbin, 1979: On the analysis of single Doppler data. *J. Appl. Meteor.*, **18**, 1521–1525.
- Woodman, R. F., 1991: A general statistical instrument theory of atmospheric and ionospheric radars. *J. Geophys. Res.*, **96**, 7911–7928.
- Xu, Q., H. Gu, and S. Yang, 2001: Simple adjoint method for three-dimensional wind retrievals from single-Doppler radar. *Quart. J. Roy. Meteor. Soc.*, **127**, 1053–1067.
- Zhang, G., R. J. Doviak, J. Vivekanandan, W. O. J. Brown, and S. A. Cohn, 2003: Cross-correlation ratio method to estimate cross-beam wind and comparison with a full correlation analysis. *Radio Sci.*, **38**, 8052, doi:10.1029/2002RS002682.
- , —, —, —, and —, 2004: Performance of correlation estimators for spaced antenna wind measurement in the presence of noise. *Radio Sci.*, **39**, RS3017, doi:10.1029/2003RS003022.
- , T.-Y. Yu, and R. J. Doviak, 2005: Angular and range interferometry to refine weather radar resolution. *Radio Sci.*, **40**, RS3013, doi:10.1029/2004RS003125.